

# Can Dark States Explain Vibropolaritonic Chemistry?

Matthew Du, Joel Yuen-Zhou\*

Department of Chemistry and Biochemistry, University of California San Diego, La Jolla, California 92093, United States

(Dated: April 22, 2021)

Collective strong coupling between a disordered ensemble of  $N$  localized molecular vibrations and a resonant optical cavity mode gives rise to 2 polariton and  $N-1 \gg 2$  dark modes. Thus, experimental changes in thermally-activated reaction kinetics due to polariton formation appear entropically unlikely and remain a puzzle. Here we show that the overlooked dark modes, while parked at the same energy as bare molecular vibrations, are robustly delocalized across  $\sim 2-3$  molecules, yielding enhanced channels of vibrational cooling, concomitantly catalyzing or suppressing a chemical reaction. As an illustration, we theoretically show a 55% increase in an electron transfer rate due to enhanced product stabilization.

The past decade has seen much interest in the control of chemical phenomena via the strong coupling of matter to confined electromagnetic modes [1–17]. An exciting prospect in this direction is vibropolaritonic chemistry, that is, the use of collective vibrational strong coupling (VSC) [18–20] to modify thermally-activated chemical reactivity without external pumping (*e.g.*, laser excitation) [21]. While collective VSC involves a large number of molecules ( $N \approx 10^6 - 10^{12}$ ) per photon mode, it has been observed to substantially alter the kinetics of organic substitution [22, 23], cycloaddition [24], hydrolysis [25], enzyme catalysis [26, 27], and crystallization [28], among other electronic ground-state chemical processes.

However, such modified reactivity under VSC is still not well understood. Studies [29–32] show that the observed kinetics cannot be explained with transition state theory (TST) [33], the most commonly used framework to predict and interpret reaction rates. Breakdowns of TST, including recrossing the activation barrier [34], deviation from thermal equilibrium [31, 35], and quantum/nonadiabatic phenomena [31, 35–38], have also been considered. The aforementioned works regard all  $N$  vibrations coupled to the cavity mode to be identical. Under this assumption, VSC forms two polaritons and  $N-1$  optically dark vibrational modes, where the latter remain unchanged from the cavity-free system. It follows that VSC-induced changes to thermally-activated reactivity must arise from the polaritons. In fact, one study from our group highlighted the molecular parameter space where polaritons dominate the kinetics [36] with respect to dark modes; however, this hypothesis has been questioned as entropically unlikely [39].

Disorder, despite its ubiquity in molecular systems, has often been ignored when modeling molecules under strong light-matter coupling. Only recently has it been shown that the strong coupling of disordered chromophores to an optical cavity mode can produce dark states which are delocalized on multiple molecules [40, 41] (hereafter, referred as semilocalized). This semilocalization is predicted to improve or even enable coherent energy transport [40, 42]. Other findings hint at adding

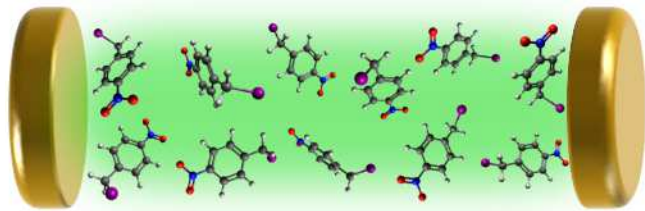


FIG. 1. Schematic of the model setup. Inside an optical cavity, a cavity mode collectively interacts with an energetically disordered ensemble of molecular vibrations, each belonging to a separate molecule. When a molecule reacts, its cavity-coupled vibrational mode concomitantly experiences a displacement in equilibrium geometry. Depicted here are molecules that undergo intramolecular electron transfer, the reaction studied in this work.

sample impurities to help strong coupling modify local molecular properties [43].

In this Letter, we demonstrate that the VSC of a disordered molecular ensemble (Fig. 1) can significantly modify the kinetics of a thermally-activated chemical reaction. The altered reactivity is attributed to the semilocalized dark modes. The semilocalization affects the reaction rate by changing the efficiency with which a reactive mode dissipates energy.

Consider a disordered ensemble of  $N$  molecular vibrations, respectively corresponding to  $N$  independent molecules, inside an optical cavity (Fig. 1). The system is described by the Hamiltonian  $H = \hbar\omega_c a_0^\dagger a_0 + \hbar \sum_{i=1}^N (\bar{\omega}_v + \delta\omega_i) a_i^\dagger a_i + \hbar \sum_{i=1}^N g_i (a_i^\dagger a_0 + \text{h.c.})$ . Vibrational mode  $i$  is represented by annihilation operator  $a_i$  and has frequency  $\bar{\omega}_v + \delta\omega_i$ , where  $\bar{\omega}_v$  is the mean vibrational frequency and  $\delta\omega_i$  is the frequency offset of mode  $i$ . Reflecting inhomogeneous broadening (static diagonal disorder),  $\delta\omega_i$  is a normally distributed random variable with mean zero and standard deviation  $\sigma_v$ . The cavity mode is represented by annihilation operator  $a_0$ , has frequency  $\omega_c$ , and couples to vibration  $i$  with strength  $g_i$ . For simplicity, we hereafter take  $g_i = g$  for all  $i$ .

Using  $H$ , we investigate the physicochemical properties of a disordered molecular system under VSC. Unless otherwise noted, calculations assume that the cav-

\* joelyuen@ucsd.edu

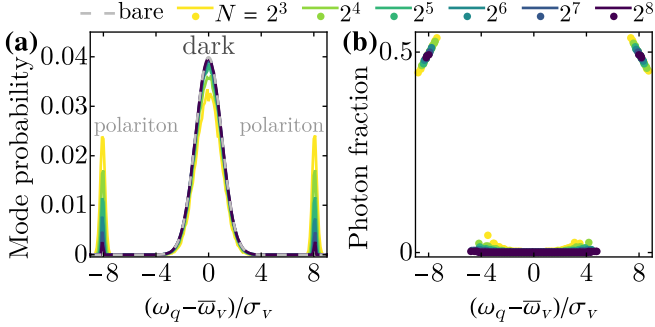


FIG. 2. (a) Probability distribution and (b) photon fraction of the eigenmodes of  $H$ . Values are plotted versus eigenfrequency  $\omega_q$  for various  $N$ . In (a), the gray dashed line is the probability density function  $[P(\omega_q) = (\sigma_v \sqrt{2\pi})^{-1} \exp(-(\omega_q - \bar{\omega}_v)^2/(2\sigma_v^2))]$ , displayed in units of  $1/\Delta\omega$  of the bare vibrational modes.

ity is resonant with the average vibration,  $\omega_c = \bar{\omega}_v$ , and couples to the vibrations with collective strength  $g\sqrt{N} = 8\sigma_v$ . Numerical values reported below are obtained by averaging over 5000 disorder realizations, *i.e.*, sets  $\{\omega_i\}_{i=1}^N$ . In plots versus the  $H$  eigenfrequencies, each data point is an average over the  $H$  eigenmodes—from all disorder realizations—whose frequency lies in the bin  $(\Delta\omega(l - \frac{1}{2}), \Delta\omega(l + \frac{1}{2})]$  for  $\Delta\omega = 10^{-1}\sigma_v$  and  $l \in \mathbb{Z}$ .

We first study the eigenmodes of  $H$ . Formally, mode  $q = 1, \dots, N + 1$  is represented by operator  $\alpha_q = \sum_{i=0}^N c_{qi} a_i$  and has frequency  $\omega_q$ . Figs. 2(a) and 2(b) show the probability distribution and photon fraction ( $|c_{q0}|^2$ ), respectively, of the eigenmodes with respect to eigenfrequency. The majority of modes form a broad distribution in frequency around  $\bar{\omega}_v$  and are optically dark. A minority of modes are polaritons, which have frequency  $\bar{\omega}_v \pm 8\sigma_v$  and photon fraction  $\approx 0.5$ . As  $N$  rises, the eigenmodes become increasingly composed of dark modes, whose probability distribution approaches that of the bare vibrational modes [Fig. 2(a), gray dashed line].

Next, we examine the delocalization of the dark modes. For the purpose of studying chemical reactions, it is useful to compute the molecular participation ratio (PR) [41, 44]. This measure, defined as

$$\text{molecular PR} = 1 / \sum_{i=1}^N \left| \frac{c_{qi}}{\sqrt{\sum_{i=1}^N |c_{qi}|^2}} \right|^4 \quad (1)$$

and analogous to the usual PR [45], estimates the number of molecules over which eigenmode  $q$  is delocalized. According to Fig. 3(a), the average dark mode has molecular PR  $\sim 2\text{-}3$ , and this semilocalization persists as  $N$  increases. These phenomena were first noted independently by Scholes [41] and Schachenmayer and co-workers [40]. For additional insight, we plot the squared overlap [ $|c_{qi}|^2$ , Fig. 3(b)] and frequency difference [ $|\omega_{qi}|$ , where  $\omega_{qi} = \omega_q - \omega_i$ ; Fig. 3(c)] between each dark mode and

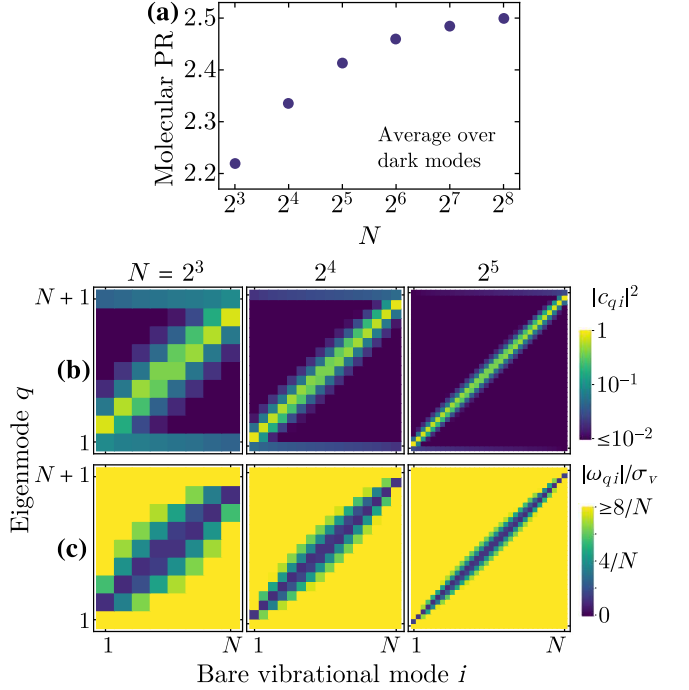


FIG. 3. (a) Average molecular PR of the dark modes as a function of  $N$ . (b) Squared overlap  $|c_{qi}|^2$  ( $\log_{10}$  scale) and (c) frequency difference  $|\omega_{qi}|$  between each eigenmode  $q$  and each bare vibrational mode  $i$ . Each group of modes is ordered from low to high frequency, *i.e.*, dark (polariton) modes have index  $q = 2, \dots, N$  ( $q = 1, N + 1$ ). The quantities in (b)-(c) are plotted for various  $N$ .

each bare vibrational mode. The typical dark mode has sizable overlap with the bare modes that are nearest to it in frequency. The frequency difference between the dark mode and any of its major constituents is  $O(\sigma_v/N)$ , *i.e.*, negligible for large  $N$ .

We now explore how VSC influences the kinetics of a thermally-activated chemical reaction. Consider a reactive molecule under collective VSC (Fig. 1). The molecule undergoes nonadiabatic intramolecular electron transfer, and a cavity mode interacts collectively with a reactive vibrational mode and  $N - 1$  nonreactive vibrational modes. The model here considered is general enough that it should also be applicable to the case of “solvent-assisted VSC” [46–49].

To model the reaction of one molecule in the ensemble, we employ the Hamiltonian  $H_{\text{rxn}} = H + \sum_{X=R,P} |X\rangle\langle X| \{E_X + \hbar\omega_r [\lambda_X (a_r + a_r^\dagger) + \lambda_X^2]\} + V + H_s^{(l)}$ . Note that vibrational and cavity modes are still described by  $H$ . In writing  $H_{\text{rxn}}$ , we have changed the numerical index of the bare vibrational mode ( $i = 1$ ) involved in the reaction to the letter  $r$  (*i.e.*,  $\omega_1 \rightarrow \omega_r$ ,  $a_1 \rightarrow a_r$ ); hereafter, we refer to this mode as  $v_r$ . The electronic subspace consists of reactant  $|R\rangle$  and product  $|P\rangle$  states. Electronic state  $|X\rangle$  has energy  $E_X$  and couples to  $v_r$  with dimensionless strength  $\lambda_X$ . As a result of the vibronic coupling,  $v_r$  experiences a displacement in its equilibrium

position upon electron transfer. The interaction between  $|R\rangle$  and  $|P\rangle$  is represented by  $V = J_{RP}(|P\rangle\langle R| + \text{h.c.})$ , where  $J_{RP}$  is the interaction strength. Through  $H_s^{(l)}$  [50], Hamiltonian  $H_{\text{rxn}}$  also accounts for low-frequency vibrational modes of the solvent that help mediate electron transfer.

Since we are considering a nonadiabatic reaction, we treat  $V$  perturbatively and calculate rates of reactive transitions between the zeroth-order electronic-vibrational-cavity eigenstates of  $H_{\text{rxn}}$ . These states take the form  $|X, \chi\rangle = |X\rangle \otimes |\tilde{\chi}_{(X)}\rangle$ . Belonging to the subspace of vibrational and cavity modes,  $|\tilde{\chi}_{(X)}\rangle = \left(\prod_{q=1}^{N+1} D_q^\dagger(\lambda_{Xq})\right) |\chi\rangle$  is a displaced Fock state with  $m_q^{(X)}$  excitations in  $H$  eigenmode  $q$ . The undisplaced Fock state  $|\chi\rangle$  is an eigenstate of  $H$ , and  $D_q(\lambda) = \exp(\lambda\alpha_q^\dagger - \lambda^*\alpha_q)$  is a displacement operator. Mode  $q$  has equilibrium (dimensionless) position  $\lambda_{Xq} = \lambda_X c_{qr}(\omega_r/\omega_q)$  when the system is in electronic state  $|X\rangle$ . Returning to the electronic-vibrational-cavity state  $|X, \chi\rangle$ , we can write its energy as  $E_{(X,\chi)} = E_X + \sum_{q=1}^{N+1} m_q^{(X)} \hbar\omega_q + \Delta_X$ , where  $\Delta_X = \lambda_X^2 \hbar\omega_r - \hbar \sum_{q=1}^{N+1} |\lambda_{Xq}|^2 \omega_q$  is the difference in reorganization energy—namely, that due to vibronic coupling between  $v_r$  and  $|X\rangle$ —with and without VSC.

Following extensions [35–37] of Marcus-Levich-Jortner theory [51–53] to electron transfer under VSC, the rate of the reactive transition from  $|R, \chi\rangle$  to  $|P, \chi'\rangle$  can be expressed as

$$k_{(R,\chi)\rightarrow(P,\chi')} = \mathcal{A}F_{\chi,\chi'} \exp\left(-\beta E_a^{\chi,\chi'}\right), \quad (2)$$

where  $\mathcal{A} = \sqrt{\pi\beta/\lambda_s} |J_{RP}|^2/\hbar$ ,  $\lambda_s$  is the reorganization energy associated with low-frequency solvent modes [50], and  $\beta$  is the inverse temperature. For this transition, the activation energy is  $E_a^{\chi,\chi'} = (E_{(P,\chi')} - E_{(R,\chi)} + \lambda_s)^2/(4\lambda_s)$ . Through the Franck-Condon (FC) factor  $F_{\chi,\chi'} = |\langle\tilde{\chi}_{(R)}|\tilde{\chi}_{(P)}'\rangle|^2$ , the transition rate depends on the overlap between initial and final vibrational-cavity states  $|\tilde{\chi}_{(R)}\rangle$  and  $|\tilde{\chi}_{(P)}'\rangle$ , respectively. It can be shown that the rate  $k_{(P,\chi')\rightarrow(R,\chi)}$  corresponding to the backward transition,  $|P, \chi'\rangle \rightarrow |R, \chi\rangle$ , is related to Eq. (2) by detailed balance [54].

We specifically study a reaction where, in the absence of light-matter coupling, reactive transitions occur on the same timescale as internal thermalization (*i.e.*, thermalization of states having the same electronic component). In such cases, internal thermal equilibrium is not maintained throughout the reaction, and the reaction rate (*i.e.*, net rate of reactant depletion) may not be approximated by a thermal average of reactant-to-product transition rates. Instead, the reaction rate can also depend on, *e.g.*, backward reactive transitions (from product to reactant) or vibrational relaxation.

With this in mind, we numerically simulate the bare ( $g = 0$ ) and VSC reactions using a kinetic model [35, 50], which includes forward and backward reactive transitions [Eq. (2)], vibrational and cavity decay, and energy exchange among dark and polariton states [55–57]. The

reaction parameters [50], which include  $\bar{\omega}_v = 2000 \text{ cm}^{-1}$  and  $\sigma_v = 10 \text{ cm}^{-1}$ , are such that the population dynamics proceeds almost completely through states  $|X, \chi\rangle$  with zero or one excitation in the vibrational-cavity modes. To reduce computational cost, the kinetic model includes only these states, which are denoted by  $\chi = 0$  and  $\chi = 1_q$ , respectively, where  $q$  is an eigenmode of the vibrational-cavity subspace. The kinetic master equation [50] is numerically solved with the initial population being a thermal distribution of reactant states ( $|R, \chi\rangle$ ). Then, the *apparent* reaction rate is obtained by fitting the reactant population as a function of time [50].

Even though we run the full numerical simulations as explained above, we now introduce approximate models that shed conceptual intuition on the calculated kinetics. First, the bare reaction can be essentially captured by Fig. 4(a), described as follows. Starting from its vibrational ground state, the reactant converts to product mainly by a  $0 \rightarrow 1$  vibronic transition, which excites the reactive mode and has rate  $k_f \equiv k_{(R,0)\rightarrow(P,1_r)}$ , where

$$k_f = \mathcal{A}F_{0,1_r} \exp(-\beta E_a), \quad (3)$$

$E_a \equiv E_a^{0,1_r}$ . The vibrationally hot product either reverts to the reactant at rate  $k_b \equiv k_{(P,1_r)\rightarrow(R,0)} \gg k_f$ , where

$$k_b = k_f \exp[\beta(E_P + \hbar\omega_r - E_R)], \quad (4)$$

or decays to its vibrational ground state at rate  $\gamma \approx k_b$ . Once the product reaches its vibrational ground state, it effectively stops reacting due to the high reverse activation energy. This kinetic scheme leads to a bare reaction rate [50]

$$k_{\text{bare}}^{(\text{analytical})} = k_f \left( \frac{\gamma}{\gamma + k_b} \right). \quad (5)$$

Second, under VSC, the primary reaction pathway of the bare case is split into multiple pathways, each involving the (de)excitation of a dark or polariton eigenmode  $q$ . For the VSC reaction channels, the forward and backward rates take the form

$$k_f^{(q)} = \mathcal{A}F_{0,1_q} \exp(-\beta E_a^{(q)}), \quad (6)$$

$$k_b^{(q)} = k_f^{(q)} \exp\{\beta [E_P + \hbar\omega_q + \Delta_P - (E_R + \Delta_R)]\}, \quad (7)$$

respectively, where  $k_f^{(q)} \equiv k_{(R,0)\rightarrow(P,1_q)}$ ,  $k_r^{(q)} \equiv k_{(P,1_q)\rightarrow(R,0)}$ , and  $E_a^{(q)} \equiv E_a^{0,1_q}$ . Now, consider the following argument, which holds strictly for large  $N$ . As  $N$  increases, the average bare mode becomes localized on dark modes that have essentially the same frequency as it [Figs. 3(b)–3(c)], and its overlap with the polariton modes vanishes [*i.e.*,  $c_{qr} \propto \frac{1}{\sqrt{N}} \rightarrow 0$  for  $q = 1, N+1$ ; see Fig. 3(b)]. These observations suggest that  $c_{qr} \not\approx 0$  only for modes  $q$  that are dark and have frequency  $\omega_q \approx \omega_r$ . It is then straightforward to show that  $E_a^{(q)} \Big|_{c_{qr} \not\approx 0} \approx E_a$ ,  $F_{0,1_q} \approx |c_{qr}|^2 F_{0,1_r}$ , and

$$k_{f/b}^{(q)} \approx |c_{qr}|^2 k_{f/b}. \quad (8)$$

Thus, VSC leads to reaction channels that have lower rates of reactive transitions, due to changes not in activation energies but in FC factors, which are smaller as a result of the semilocalization of dark modes. From Eq. (8), it is evident that the total forward rate is approximately that of the bare reaction ( $\sum_{q=1}^{N+1} k_f^{(q)} \approx k_f$ , since  $\sum_{q=1}^{N+1} |c_{qr}|^2 = 1$ ). However, once a forward reactive transition happens—and a dark mode is excited—the product either returns to the reactant at a *reduced rate* ( $k_b^{(q)} < k_b$ ) or, due to the almost fully vibrational nature of the dark modes, vibrationally decays to its stable form ( $|P, 0\rangle$ ) at essentially the same *bare rate* ( $\gamma$ ). In other words, VSC suppresses reverse reactive transitions by promoting the cooling of the reactive mode upon product formation. In analogy to Eq. (5), we determine an effective rate for the VSC reaction [50]:

$$k_{\text{VSC}}^{(\text{analytical})} = k_f \left\langle \frac{\gamma}{\gamma + |c_{qr}|^2 k_b} \right\rangle_{\text{dark modes } q}, \quad (9)$$

where  $\langle \cdot \rangle_{\text{dark modes } q}$  is a weighted average over all dark modes  $q$ , each with weight  $|c_{qr}|^2$ . Since  $|c_{qr}|^2 < 1$  for all  $q$ , then  $k_{\text{VSC}}^{(\text{analytical})} > k_{\text{bare}}^{(\text{analytical})}$ . We emphasize that the major contributions to the average in Eq. (9) come from dark modes which are closest in frequency to the bare reactive mode (see above). Further enhancement of the VSC reaction, beyond that given by  $k_{\text{VSC}}^{(\text{analytical})}$ , occurs via dissipative scattering from these dark modes to those with  $c_{qr} \approx 0$ . Said differently, the product is protected from reversion to reactant when dark modes with relatively more reactive character lose their energy to those with relatively less. The VSC reaction kinetics, as described above, is summarized in Fig. 4(b).

Fig. 4(e) shows the ratio of VSC reaction rate to bare reaction rate, as determined from numerical kinetic simulations. As we have shown analytically, VSC significantly accelerates the reaction compared to the bare case. As  $N$  increases, the rate enhancement [Fig. 4(e), purple filled circles] converges to approximately 55%; hence, despite our computational simulations capping at  $N = 2^8$ , we expect this behavior and the subsequent analysis to hold for the experimentally relevant  $N = 10^6 - 10^{12}$ . Interestingly, the rate enhancement follows the same  $N$ -dependence as the reactive-mode delocalization, which is shown in Fig. 4(d) and defined as  $1 / \sum_{q=1}^{N+1} |c_{qr}|^4$  (the PR of  $v_r$  when the mode is expressed in the eigenbasis of  $H$ ). This correlation supports that, for many-molecule VSC, the reaction proceeds through the dark modes and is enhanced by their semilocalization. The present scenario is quite generic and contrasts with our previous model where extreme geometric parameters are needed for polaritons to dominate the VSC kinetics [36]. Indeed, the reaction here is unaffected by cavity leakage when  $N$  is sufficiently large [50].

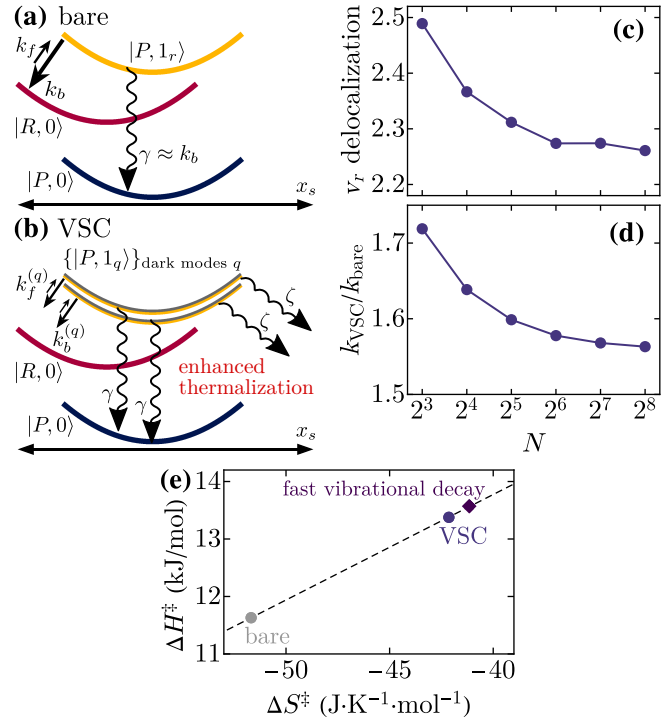


FIG. 4. (a) Schematic of the bare reaction kinetics. Parabolas represent potential energy surfaces with respect to the effective low-frequency coordinate  $x_s$ . After a reactive transition ( $|R, 0\rangle \rightarrow |P, 1_r\rangle$ ) with rate  $k_f$ , the product either reverts to the reactant ( $|P, 1_r\rangle \rightarrow |R, 0\rangle$ ) at rate  $k_b$  or vibrationally decays to its stable form ( $|P, 1_r\rangle \rightarrow |P, 0\rangle$ ) at rate  $\gamma \approx k_b$ . (b) Schematic of the reaction kinetics under VSC. The half-yellow half-gray parabolas qualitatively represent potential energy surfaces of product states with one excitation in a dark mode ( $|P, 1_q\rangle$ ). The reaction proceeds via multiple reaction channels, each involving a reactive transition ( $|R, 0\rangle \rightarrow |P, 1_q\rangle$ ) with rate  $k_f^{(q)} < k_f$  to the product with one excitation in a dark mode. The total forward rate is approximately the bare rate  $k_f$ . In contrast, the vibrationally hot product formed from each reaction channel either returns to the reactant ( $|P, 1_q\rangle \rightarrow |R, 0\rangle$ ) at rate  $k_b^{(q)} < k_b$  or cools ( $|P, 1_q\rangle \rightarrow |P, 0\rangle$ ) at the *bare* molecular rate  $\gamma$ . There is also scattering (at effective rate  $\zeta$ ) from dark modes with  $c_{qr} \neq 0$  to those with  $c_{qr} \approx 0$ . Overall, VSC accelerates product thermalization, suppressing backward reactive transitions, and thus enhancing the net reaction rate. (c)  $v_r$  delocalization and (d)  $k_{\text{VSC}}/k_{\text{bare}}$  as a function of  $N$ . (e) Activation enthalpy  $\Delta H^\ddagger$  versus activation entropy  $\Delta S^\ddagger$  for reactions with  $N = 2^8$ : bare (gray circle), VSC (purple circle), and bare with vibrational decay rate  $\gamma$  made 100 times faster (purple diamond). The black dashed line is a fit to the points shown. In (d) and (e), the individual rates ( $k_{\text{VSC}}, k_{\text{bare}}$ ) and thermodynamic parameters ( $\Delta H^\ddagger, \Delta S^\ddagger$ ) are averages over 5000 disorder realizations.

For additional mechanistic insight into VSC catalysis and following the procedures in [22, 24, 46], we plot in Fig. 4(f) the activation enthalpy ( $\Delta H^\ddagger$ ) versus activation entropy ( $\Delta S^\ddagger$ ) for multiple cases of VSC and bare reactions. The thermodynamic parameters of activation are computed by calculating the apparent reaction rate for

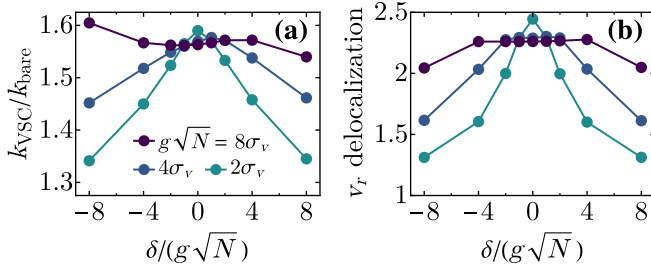


FIG. 5. (a)  $kvSC/k_{\text{bare}}$  and (b)  $v_r$  delocalization, as a function of cavity detuning  $\delta$ , for various collective light-matter coupling strengths  $g\sqrt{N}$  and fixed  $N = 2^8$ . In (a),  $kvSC$  is an average over 5000 disorder realizations, and  $k_{\text{bare}}$  is a value used to obtain Fig. 4(d).

additional temperatures and fitting the obtained values to the Eyring-Polanyi equation [50]. This fit indicates that changes in effective parameters  $\Delta H^\ddagger$  and  $\Delta S^\ddagger$  can result from dynamical effects such as accelerated vibrational decay, rather than from potential energy changes.

The deduced connection between reactivity under VSC and reactive-mode delocalization is corroborated by their dependence on cavity detuning  $\delta = \omega_c - \bar{\omega}_v$  (Fig. 5). We find, for various light-matter coupling strengths, that the reactive-mode delocalization is maximum close to resonance and eventually decreases with detuning. The rate enhancement due to VSC mostly follows the same trend. Any major deviation from this trend is attributed to the polaritons and expected to vanish if  $N$  is sufficiently increased [50], since extreme molecular geometries are not considered [36].

In conclusion, we show that, by forming semilocalized

dark modes, the VSC of a disordered molecular ensemble can modify the kinetics of a thermally-activated chemical reaction. For a reactive molecule under collective VSC, we find that the electron transfer rate is significantly increased. The spreading of reactive character across dark modes, as well as the dissipative scattering among these modes, allows the reactive mode to thermalize more efficiently once the product is formed, suppressing dynamical effects, such as reversion to reactant. Finally, while we study a nonadiabatic reaction, our main conclusions are general and should be relevant for the understanding of adiabatic reactions under VSC (work in progress). More broadly, our work highlights that the previously overlooked dark states are the entropically likely channels through which collective light-matter interaction can control chemistry.

## ACKNOWLEDGMENTS

We are grateful to Jorge Campos-Gonzalez-Angulo, Arghadip Koner, Luis Martínez-Martínez, Kai Schwennicke, Stephan van den Wildenberg, and Garret Wiesehan for useful discussions. This work employed computational resources of the Extreme Science and Engineering Discovery Environment (XSEDE), which is supported by National Science Foundation Grant No. ACI-1548562, under allocation No. TG-ASC150024. We also thank Marty Kandes and Nicole Wolter for assistance in using these resources. Acknowledgment is made to the donors of The American Chemical Society Petroleum Research Fund for partial support of this research through the ACS PRF 60968-ND6 award. M.D. is also supported by a UCSD Roger Tsien Fellowship.

---

[1] V. M. Agranovich, Y. N. Gartstein, and M. Litinskaya, *Chem. Rev.* **111**, 5179 (2011).

[2] D. M. Coles, N. Somaschi, P. Michetti, C. Clark, P. G. Lagoudakis, P. G. Savvidis, and D. G. Lidzey, *Nat. Mater.* **13**, 712 (2014).

[3] T. W. Ebbesen, *Acc. Chem. Res.* **49**, 2403 (2016).

[4] M. Kowalewski, K. Bennett, and S. Mukamel, *J. Phys. Chem. Lett.* **7**, 2050 (2016).

[5] R. Chikkaraddy, B. de Nijs, F. Benz, S. J. Barrow, O. A. Scherman, E. Rosta, A. Demetriadou, P. Fox, O. Hess, and J. J. Baumberg, *Nature* **535**, 127 (2016).

[6] J. Feist, J. Galego, and F. J. Garcia-Vidal, *ACS Photonics* **5**, 205 (2017).

[7] B. Barnes, F. García Vidal, and J. Aizpurua, *ACS Photonics* **5**, 1 (2018).

[8] F. Herrera and F. C. Spano, *ACS Photonics* **5**, 65 (2018).

[9] D. G. Baranov, M. Wersäll, J. Cuadra, T. J. Antosiewicz, and T. Shegai, *ACS Photonics* **5**, 24 (2018).

[10] R. F. Ribeiro, L. A. Martínez-Martínez, M. Du, J. Campos-Gonzalez-Angulo, and J. Yuen-Zhou, *Chem. Sci.* **9**, 6325 (2018).

[11] J. Flick, N. Rivera, and P. Narang, *Nanophotonics* **7**, 1479 (2018).

[12] M. Hertzog, M. Wang, J. Mony, and K. Börjesson, *Chem. Soc. Rev.* **48**, 937 (2019).

[13] F. Herrera and J. Owrusky, *J. Chem. Phys.* **152**, 100902 (2020).

[14] E. Coccia, J. Fregoni, C. A. Guido, M. Marsili, S. Pipolo, and S. Corni, *J. Chem. Phys.* **153**, 200901 (2020).

[15] N. M. Hoffmann, L. Lacombe, A. Rubio, and N. T. Maitra, *J. Chem. Phys.* **153**, 104103 (2020).

[16] P. Antoniou, F. Suchanek, J. F. Varner, and J. J. Foley, *J. Phys. Chem. Lett.* **11**, 9063 (2020).

[17] T. S. Haugland, E. Ronca, E. F. Kjønstad, A. Rubio, and H. Koch, *Phys. Rev. X* **10**, 041043 (2020).

[18] A. Shalabney, J. George, J. Hutchison, G. Pupillo, C. Genet, and T. W. Ebbesen, *Nat. Commun.* **6**, 6 (2015).

[19] J. P. Long and B. S. Simpkins, *ACS Photonics* **2**, 130 (2015).

[20] S. R. Casey and J. R. Sparks, *J. Phys. Chem. C* **120**, 28138 (2016).

[21] K. Hirai, J. A. Hutchison, and H. Uji-i, *ChemPlusChem* **85**, 1981 (2020).

[22] A. Thomas, J. George, A. Shalabney, M. Dryzhakov, S. J. Varma, J. Moran, T. Chervy, X. Zhong, E. Devaux, C. Genet, J. A. Hutchison, and T. W. Ebbesen, *Angew. Chem., Int. Ed.* **128**, 11634 (2016).

[23] A. Thomas, L. Lethuillier-Karl, K. Nagarajan, R. M. A. Vergauwe, J. George, T. Chervy, A. Shalabney, E. Devaux, C. Genet, J. Moran, and T. W. Ebbesen, *Science* **363**, 615 (2019).

[24] K. Hirai, R. Takeda, J. A. Hutchison, and H. Uji-i, *Angew. Chem., Int. Ed.* **132**, 5370 (2020).

[25] H. Hiura, A. Shalabney, and J. George, *ChemRxiv* (2019).

[26] R. M. A. Vergauwe, A. Thomas, K. Nagarajan, A. Shalabney, J. George, T. Chervy, M. Seidel, E. Devaux, V. Torbeev, and T. W. Ebbesen, *Angew. Chem., Int. Ed.* **58**, 15324 (2019).

[27] J. Lather and J. George, *J. Phys. Chem. Lett.* **12**, 379 (2021).

[28] K. Hirai, H. Ishikawa, J. Hutchison, and H. Uji-i, *ChemRxiv* (2020).

[29] J. Galego, C. Climent, F. J. Garcia-Vidal, and J. Feist, *Phys. Rev. X* **9**, 021057 (2019).

[30] J. A. Campos-Gonzalez-Angulo and J. Yuen-Zhou, *J. Chem. Phys.* **152**, 161101 (2020).

[31] T. E. Li, A. Nitzan, and J. E. Subotnik, *J. Chem. Phys.* **152**, 234107 (2020).

[32] V. P. Zhdanov, *Chem. Phys.* **535**, 110767 (2020).

[33] P. Hänggi, P. Talkner, and M. Borkovec, *Rev. Mod. Phys.* **62**, 251 (1990).

[34] X. Li, A. Mandal, and P. Huo, *Nat. Commun.* **12**, 1315 (2021).

[35] M. Du, J. A. Campos-Gonzalez-Angulo, and J. Yuen-Zhou, *J. Chem. Phys.* **154**, 084108 (2021).

[36] J. A. Campos-Gonzalez-Angulo, R. F. Ribeiro, and J. Yuen-Zhou, *Nat. Commun.* **10**, 4685 (2019).

[37] N. T. Phuc, P. Q. Trung, and A. Ishizaki, *Sci. Rep.* **10**, 7318 (2020).

[38] E. W. Fischer and P. Saalfrank, *J. Chem. Phys.* **154**, 104311 (2021).

[39] I. Vurgaftman, B. S. Simpkins, A. D. Dunkelberger, and J. C. Owrusky, *J. Phys. Chem. Lett.* **11**, 3557 (2020).

[40] T. Botzung, D. Hagenmüller, S. Schütz, J. Dubail, G. Pupillo, and J. Schachenmayer, *Phys. Rev. B* **102**, 144202 (2020).

[41] G. D. Scholes, *Proc. R. Soc. A* **476**, 20200278 (2020).

[42] N. C. Chávez, F. Mattiotti, J. A. Méndez-Bermúdez, F. Borgonovi, and G. L. Celardo, *Phys. Rev. Lett.* **126**, 153201 (2021).

[43] D. Sidler, C. Schäfer, M. Ruggenthaler, and A. Rubio, *J. Phys. Chem. Lett.* **12**, 508 (2021).

[44] J. Galego, F. J. Garcia-Vidal, and J. Feist, *Phys. Rev. Lett.* **119**, 136001 (2017).

[45] B. Kramer and A. MacKinnon, *Rep. Prog. Phys.* **56**, 1469 (1993).

[46] J. Lather, P. Bhatt, A. Thomas, T. W. Ebbesen, and J. George, *Angew. Chem., Int. Ed.* **58**, 10635 (2019).

[47] S. Schütz, J. Schachenmayer, D. Hagenmüller, G. K. Brennen, T. Volz, V. Sandoghdar, T. W. Ebbesen, C. Genes, and G. Pupillo, *Phys. Rev. Lett.* **124**, 113602 (2020).

[48] T. Szidarovszky, G. J. Halász, and A. Vibók, *New J. Phys.* **22**, 053001 (2020).

[49] E. Davidsson and M. Kowalewski, *J. Phys. Chem. A* **124**, 4672 (2020).

[50] See Supplemental Material at [URL will be inserted by publisher] for Hamiltonian  $H_s^{(l)}$ , kinetic model, parameters and numerical methods for calculating reaction rates, procedure to determine thermodynamic parameters of activation, derivations of analytical reaction rates, and supplemental figures.

[51] R. A. Marcus, *Annu. Rev. Phys. Chem.* **15**, 155 (1964).

[52] V. G. Levich, *Adv. Electrochem. Electrochem. Eng.* **4**, 249 (1966).

[53] J. Jortner, *J. Chem. Phys.* **64**, 4860 (1976).

[54] O. Kühn and H. Naundorf, *Phys. Chem. Chem. Phys.* **5**, 79 (2003).

[55] J. del Pino, J. Feist, and F. J. Garcia-Vidal, *New J. Phys.* **17**, 053040 (2015).

[56] B. Xiang, R. F. Ribeiro, A. D. Dunkelberger, J. Wang, Y. Li, B. S. Simpkins, J. C. Owrusky, J. Yuen-Zhou, and W. Xiong, *Proc. Natl. Acad. Sci. U. S. A.* **115**, 4845 (2018).

[57] B. Xiang, R. F. Ribeiro, L. Chen, J. Wang, M. Du, J. Yuen-Zhou, and W. Xiong, *J. Phys. Chem. A* **123**, 5918 (2019).

# Supplemental Material: Can Dark States Explain Vibropolaritonic Chemistry?

Matthew Du, Joel Yuen-Zhou\*

Department of Chemistry and Biochemistry, University of California San Diego, La Jolla, California 92093, United States

(Dated: April 22, 2021)

## I. HAMILTONIAN $H_s^{(l)}$

The Hamiltonian  $H_s^{(l)}$ , which is the last term of Hamiltonian  $H_{\text{rxn}}$  (defined in main text), describes the low-frequency vibrational modes of the solvent that help mediate electron transfer. We define the former Hamiltonian as

$$H_s^{(l)} = \hbar \sum_j \omega_j^{(l)} b_j^\dagger b_j + \hbar \sum_j \omega_j^{(l)} \sum_{X=R,P} |X\rangle \langle X| \left[ \lambda_{Xj}^{(l)} (b_j + b_j^\dagger) + (\lambda_{Xj}^{(l)})^2 \right],$$

where the  $j$ th low-frequency mode has frequency  $\omega_j^{(l)}$  and couples to electronic state  $|X\rangle$  with dimensionless strength  $\lambda_{Xj}$ . The contribution of the low-frequency modes to the reaction rate is characterized by reorganization energy  $\lambda_s = \sum_j (\lambda_{Pj}^{(l)} - \lambda_{Rj}^{(l)})^2 \hbar \omega_j^{(l)}$ .

## II. KINETIC MODEL

Here, we describe in detail the kinetic model used to simulate the reaction. As discussed in the main text, this model only considers states  $|X, \chi\rangle$  whose vibrational-cavity component has zero ( $\chi = 0$ ) or one ( $\chi = 1_q$ , where  $q = 1, \dots, N+1$ ) excitation. The population  $p_{(X,\chi)}$  of state  $|X, \chi\rangle$  evolves according to the master equation

$$\frac{dp_{(X,\chi)}}{dt} = - \sum_{(X',\chi') \neq (X,\chi)} k_{(X,\chi) \rightarrow (X',\chi')} p_{(X,\chi)} + \sum_{(X',\chi') \neq (X,\chi)} k_{(X',\chi') \rightarrow (X,\chi)} p_{(X',\chi')}. \quad (\text{S1})$$

State-to-state transitions ( $|X, \chi\rangle \rightarrow |X', \chi'\rangle$ ) are either reactive ( $X' \neq X$ ) or nonreactive ( $X' = X$ ).

Rates ( $k_{(X,\chi) \rightarrow (X',\chi')}$  for  $X' \neq X$ ) of reactive transitions are given by Eq. (2) and depend on FC factor  $F_{\chi,\chi'}$ , which is defined in the main text. We now evaluate  $F_{\chi,\chi'}$  for various combinations of  $\chi$  and  $\chi'$ . Recall the standard identity [S1]

$$\langle m' | D(\lambda) | m \rangle = \sqrt{\frac{m!}{(m')!}} e^{-|\lambda|^2/2} \lambda^{m'-m} L_m^{(m'-m)}(|\lambda|^2), \quad m' \geq m, \quad (\text{S2})$$

where  $D(\lambda) = \exp(\lambda a^\dagger - \lambda^* a)$  is the displacement operator corresponding to bosonic annihilation operator  $a$ ,  $|m\rangle$  is a number state of the mode represented by  $a$ , and  $L_n^k(x)$  is an associated Laguerre polynomial. Using Eq. (S2), we obtain

$$F_{\chi,\chi'} = \begin{cases} e^{-S}, & (\chi', \chi) = (0, 0), \\ e^{-S} S_q, & (\chi', \chi) = (1_q, 0), (0, 1_q), \\ e^{-S} (1 - S_q)^2, & (\chi', \chi) = (1_q, 1_q), \\ e^{-S} S_{q'} S_q, & (\chi', \chi) = (1_{q'}, 1_q), \quad q' \neq q, \end{cases} \quad (\text{S3})$$

where  $S = \sum_{q=1}^{N+1} S_q$  and  $S_q = |\lambda_{Pq} - \lambda_{Rq}|^2$ .

The nonreactive transitions in our model are of two types: (1) decay/gain of an excitation in vibrational-cavity mode  $q$  and (2) energy exchange among dark and polariton states. An excitation in mode  $q$  decays at rate

$$k_{(X,1_q) \rightarrow (X,0)} = |c_{q0}|^2 \kappa + \left( \sum_{i=1}^N |c_{qi}|^2 \right) \gamma, \quad (\text{S4})$$

\* joelyuen@ucsd.edu

where  $\kappa$  is the decay (leakage) rate of the bare cavity and  $\gamma$  is the decay rate of all bare vibrations. Detailed balance governs the rate of the reverse process:  $k_{(X,0)\rightarrow(X,1_q)} = k_{(X,1_q)\rightarrow(X,0)} \exp(-\beta\hbar\omega_q)$ . Relaxation among dark and polariton states is driven by anharmonic coupling between bare molecular vibrations and their local chemical environment [S2–S4]. Following theories [S2, S5, S6] of relaxation dynamics for molecules under VSC, the transition from a polariton or dark state to another has rate

$$k_{(X,1_q)\rightarrow(X,1_{q'})} = 2\pi \left( \sum_{i=1}^N |c_{q'i}|^2 |c_{qi}|^2 \right) [\Theta(-\omega) (n(-\omega) + 1) J(-\omega) + \Theta(\omega) n(\omega) J(\omega)], \quad (\text{S5})$$

where  $q' \neq q$  and  $\Theta(\omega)$  is the Heaviside step function. The environmental modes are characterized by spectral density  $J(\omega)$  and the Bose-Einstein distribution function,  $n(\omega) = (\exp(\beta\hbar\omega) - 1)^{-1}$ .

### III. DEFAULT PARAMETERS FOR CALCULATIONS OF REACTION RATE

Unless otherwise stated, calculations of reaction rates are carried out using the parameters described in this section. For the bare molecular vibrations, we choose a mean frequency of  $\bar{\omega}_v = 2000 \text{ cm}^{-1}$ , which is representative of experimental studies on VSC [S3, S4, S7–S10]. Since these studies do not report values of inhomogeneous broadening, we simply take the vibrational frequencies to have a standard deviation of  $\sigma_v = 10 \text{ cm}^{-1}$ . This choice of  $\sigma_v$  yields a spectral linewidth of  $\approx 24 \text{ cm}^{-1}$ , which is consistent with vibrational lineshapes measured in some of the cited works [S4, S8–S10]. Regarding the electronic degree of freedom and its coupling to other degrees of freedom, we select parameters employed in the reaction simulations of [S11]:  $E_R = 0$ ,  $E_P = -0.6\bar{\omega}_v$ ,  $\lambda_R = 0$ ,  $\lambda_P = 1.5$ ,  $J_{RP} = 0.01\bar{\omega}_v$ ,  $\lambda_s = 0.08\bar{\omega}_v$ .

Next, we describe the parameters governing the relaxation of vibrational and cavity modes. The temperature  $T$  is set to 298 K. We choose  $\kappa = 1 \text{ ps}^{-1}$  as the bare cavity decay rate and  $\gamma = 0.01 \text{ ps}^{-1}$  for the decay rate of all bare vibrational modes [S4]. To model the relaxation among dark and polariton states [Eq. (S5)], we use the Ohmic spectral density  $J(\omega) = \eta\omega \exp(-\omega/\omega_{\text{cut}})$ , where  $\eta = 2 \times 10^{-3}$  is the interaction strength between each bare vibrational mode and its local chemical environment, and  $\omega_{\text{cut}} = 50 \text{ cm}^{-1}$  is the cutoff frequency of the environmental modes. The chosen spectral density resembles those in models of liquid-phase molecular systems [S12–S14].

### IV. NUMERICAL KINETIC SIMULATIONS AND RATE CALCULATIONS

In this section, we first describe our numerical simulations of the reaction kinetics. We then discuss how we obtain the reaction rate from the numerically determined reactant population versus time. To be clear, we note that the quantities (e.g., populations, energies) shown below pertain only to states with  $\chi = 0, 1_q$  for  $q = 1, \dots, N+1$  (see main text).

State populations as a function of time are simulated by numerically solving master equation (S1). We start by writing the equation as  $d\mathbf{p}/dt = A\mathbf{p}$ , where  $\mathbf{p}$  is the vector of populations and  $A$  is the matrix of transition rates. Subsequently, we apply the following standard procedure to evaluate  $\mathbf{p}(t) = \exp(At)\mathbf{p}(0)$  [S15]. This method employs the symmetrization of  $A$  to avoid a numerically unstable matrix inversion. First, we compute the matrix  $B = MAM^{-1}$ , where  $M$  is the diagonal matrix with diagonal elements  $M_{(X,\chi),(X,\chi)} = f_{(X,\chi)}^{-1/2}$ , and  $f_{(X,\chi)} = \exp(-\beta E_{(X,\chi)}) / \sum_{(X,\chi)} \exp(-\beta E_{(X,\chi)})$ . Since the transition rates [Eqs. (2), (S4)–(S5)] satisfy detailed balance,  $B$  is symmetric. After numerically diagonalizing  $B$ , the population at time  $t$  is evaluated as

$$\mathbf{p}(t) = M^{-1}Q \exp(Dt)Q^\top M \mathbf{p}(0), \quad (\text{S6})$$

where  $Q$  is a matrix whose columns are the eigenvectors of  $B$ ,  $D$  is the diagonal matrix whose diagonal elements are the eigenvalues corresponding to said eigenvectors, and  $Q^\top = Q^{-1}$  due to  $B$  being symmetric. Because we are interested in thermally activated reactivity, the vector of initial populations,  $\mathbf{p}(0)$ , is taken to be a thermal distribution of reactant eigenstates:

$$p_{(R,\chi)}(0) = \frac{\exp(-\beta E_{(R,\chi)})}{\sum_\chi \exp(-\beta E_{(R,\chi)})}, \quad (\text{S7a})$$

$$p_{(P,\chi)}(0) = 0. \quad (\text{S7b})$$

We evaluate  $\mathbf{p}(t)$  at  $t = j\Delta t$ , where  $\Delta t = 0.2 \text{ ns}$  and  $j = 0, \dots, 100$ .

Next, the reaction rate is obtained by fitting the numerically determined values of reactant population,

$$p_R = \sum_{\chi} p_{(R,\chi)}, \quad (\text{S8})$$

and their respective values of  $t$  to the exponential function

$$p_R = \exp(-kt). \quad (\text{S9})$$

The fitting parameter  $k$  is the reaction rate. For all fits, the adjusted  $R^2$  values have mean 0.99999 and standard deviation  $8 \times 10^{-6}$ . Such successful fitting reflects the reaction being first-order [S16] in reactant. Here, first-order kinetics occurs because product excited states do not accumulate sufficiently (see §V) and the product ground state does not revert to reactant states at a fast enough rate (due to high activation energy).

## V. ANALYTICAL RATE: BARE REACTION

A simplified kinetic model for the bare reaction is shown in Fig. 4(a). In this model, the populations of  $|R, 0\rangle$  and  $|P, 1_r\rangle$  evolve as

$$\frac{dp_{(R,0)}}{dt} = -k_f p_{(R,0)} + k_b p_{(P,1_r)}, \quad (\text{S10})$$

$$\frac{dp_{(P,1_r)}}{dt} = -(k_b + \gamma) p_{(P,1_r)} + k_f p_{(R,0)}, \quad (\text{S11})$$

respectively. Since  $k_f \ll k_b, \gamma$  (see main text),  $p_{(P,1_r)}$  does not accumulate, and so we apply the steady-state approximation (SSA) [S16] to this population:  $dp_{(P,1_r)}/dt \approx 0$ . Solving the resulting equation for  $p_{(P,1_r)}$  and plugging the solution into Eq. (S10) leads to  $dp_{(R,0)}/dt \approx -k_{\text{bare}}^{(\text{analytical})} p_{(R,0)}$ . Defined in Eq. (5),  $k_{\text{bare}}^{(\text{analytical})} = k_f \left( \frac{\gamma}{\gamma + k_b} \right)$  represents the net rate of reactant depletion, *i.e.*, the reaction rate.

## VI. ANALYTICAL RATE: VSC REACTION

Here, we consider a simplified kinetic model for the VSC reaction. In this model, polaritons are decoupled from the reaction, and the reaction proceeds through multiple reaction channels, each involving the (de)excitation of a dark mode. Define  $\mathcal{D}$  as the set of dark modes. The populations of  $|R, 0\rangle$  and  $|P, 1_q\rangle$ , where  $q \in \mathcal{D}$ , evolve according to

$$\frac{dp_{(R,0)}}{dt} = - \sum_{q \in \mathcal{D}} k_f^{(q)} p_{(R,0)} + \sum_{q \in \mathcal{D}} k_b^{(q)} p_{(P,1_q)}, \quad (\text{S12})$$

$$\frac{dp_{(P,1_q)}}{dt} = - \left( k_b^{(q)} + \gamma \right) p_{(P,1_q)} + k_f^{(q)} p_{(R,0)}, \quad (\text{S13})$$

respectively. In analogy to the derivation of §V, we can apply the SSA to each  $p_{(P,1_q)}$  to arrive at

$$\frac{dp_{(R,0)}}{dt} \approx -k_f \left( \sum_{q \in \mathcal{D}} |c_{qr}|^2 \frac{\gamma}{\gamma + |c_{qr}|^2 k_b} \right) p_{(R,0)}, \quad (\text{S14})$$

where we have used Eq. (8). Eq (S14) is equivalent to  $dp_{(R,0)}/dt \approx -k_{\text{VSC}}^{(\text{analytical})} p_{(R,0)}$ , where the reaction rate constant  $k_{\text{VSC}}^{(\text{analytical})} = k_f \left( \sum_{q \in \mathcal{D}} |c_{qr}|^2 \frac{\gamma}{\gamma + |c_{qr}|^2 k_b} \right)$  is equivalent to that shown in Eq. (9) the main text.

## VII. THERMODYNAMIC PARAMETERS OF ACTIVATION

To determine the thermodynamic parameters of activation for a given reaction (*i.e.*, set of reaction parameters excluding temperature,  $T$ ), we calculate the reaction rate,  $k$ , for  $T = 273, 283, 288, 293, 298$  K. The rates are

computed using numerical kinetic simulations, as described in §IV. We then fit the  $(k, T)$  values to the Eyring-Polanyi equation [S17, S18],

$$k = \frac{k_B T}{h} \exp \left( -\frac{\Delta H^\ddagger}{RT} + \frac{\Delta S^\ddagger}{R} \right), \quad (\text{S15})$$

where  $R$  is the gas constant. The fitting parameters  $\Delta H^\ddagger$  and  $\Delta S^\ddagger$  are the enthalpy and entropy, respectively, of activation.

For all fits, the adjusted  $R^2$  values have mean  $0.999999$  and standard deviation  $2 \times 10^{-7}$ . This excellent agreement between the numerically obtained rates and the Eyring-Polanyi equation is attributed to a fortuitous choice of temperature range over which the fittings are performed. Suboptimal goodness of fit is expected for general ranges of  $T$  because the transition rates [Eqs. (2), (S4)-(S5)] of our kinetic model have a different functional form (with respect to  $T$ ) compared to Eq. (S15).

## VIII. SUPPLEMENTAL FIGURES

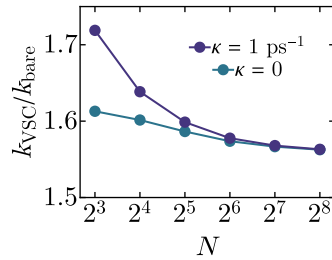


FIG. S1.  $k_{\text{VSC}}/k_{\text{bare}}$  as a function of  $N$  for various cavity leakage rates ( $\kappa$ ). The plotted values are ratios of rates ( $k_{\text{VSC}}, k_{\text{bare}}$ ), where each rate is an average over 5000 disorder realizations. The data corresponding to  $\kappa = 1 \text{ ps}^{-1}$  is the same as that in Fig. 4(d).

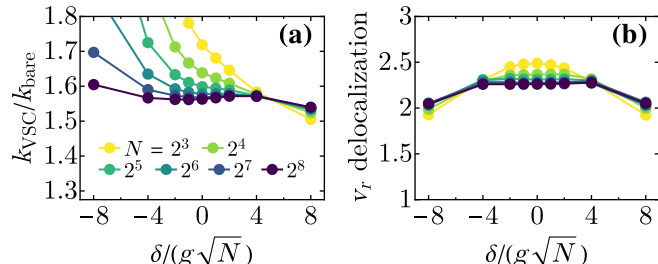


FIG. S2. (a)  $k_{\text{VSC}}/k_{\text{bare}}$  and (b)  $v_r$  delocalization, as a function of cavity detuning  $\delta$ , for various  $N$  and fixed collective light-matter coupling strength  $g\sqrt{N} = 8\sigma_v$ . In (a),  $k_{\text{VSC}}$  is an average over 5000 disorder realizations, and  $k_{\text{bare}}$  is a value used to obtain Fig. 4(d). As  $N$  increases, the  $\delta$ -dependence of  $k_{\text{VSC}}/k_{\text{bare}}$  becomes more similar to that of  $v_r$  delocalization.

---

[S1] G. Agarwal, *Quantum Optics* (Cambridge University Press, 2013).  
 [S2] J. del Pino, J. Feist, and F. J. Garcia-Vidal, *New J. Phys.* **17**, 053040 (2015).  
 [S3] B. Xiang, R. F. Ribeiro, A. D. Dunkelberger, J. Wang, Y. Li, B. S. Simpkins, J. C. Owrtusky, J. Yuen-Zhou, and W. Xiong, *Proc. Natl. Acad. Sci. U. S. A.* **115**, 4845 (2018).  
 [S4] B. Xiang, R. F. Ribeiro, L. Chen, J. Wang, M. Du, J. Yuen-Zhou, and W. Xiong, *J. Phys. Chem. A* **123**, 5918 (2019).  
 [S5] V. M. Agranovich, M. Litinskaya, and D. G. Lidzey, *Phys. Rev. B* **67**, 085311 (2003).  
 [S6] M. Litinskaya, P. Reineker, and V. M. Agranovich, *J. Lumin.* **110**, 364 (2004).  
 [S7] A. D. Dunkelberger, B. T. Spann, K. P. Fears, B. S. Simpkins, and J. C. Owrtusky, *Nat. Commun.* **7**, 13504 (2016).  
 [S8] J. Lather, P. Bhatt, A. Thomas, T. W. Ebbesen, and J. George, *Angew. Chem., Int. Ed.* **58**, 10635 (2019).

- [S9] K. Hirai, R. Takeda, J. A. Hutchison, and H. Uji-i, *Angew. Chem., Int. Ed.* **132**, 5370 (2020).
- [S10] A. B. Grafton, A. D. Dunkelberger, B. S. Simpkins, J. F. Triana, F. J. Hernández, F. Herrera, and J. C. Owrtusky, *Nat. Commun.* **12**, 214 (2021).
- [S11] M. Du, J. A. Campos-Gonzalez-Angulo, and J. Yuen-Zhou, *J. Chem. Phys.* **154**, 084108 (2021).
- [S12] Y. J. Chang and E. W. Castner, *J. Chem. Phys.* **99**, 7289 (1993).
- [S13] P. Vöhringer, D. C. Arnett, R. A. Westervelt, M. J. Feldstein, and N. F. Scherer, *J. Chem. Phys.* **102**, 4027 (1995).
- [S14] O. Kühn and H. Naundorf, *Phys. Chem. Chem. Phys.* **5**, 79 (2003).
- [S15] T. J. Frankcombe and S. C. Smith, *Comput. Phys. Commun.* **141**, 39 (2001).
- [S16] P. Atkins and J. de Paula, *Physical Chemistry*, 9th ed. (OUP Oxford, 2010).
- [S17] H. Eyring, *J. Chem. Phys.* **3**, 107 (1935).
- [S18] M. G. Evans and M. Polanyi, *Trans. Faraday Soc.* **31**, 875 (1935).